



This is a repository copy of *pH-Responsive diblock copolymers with two different fluorescent labels for simultaneous monitoring of micellar self-assembly and degree of protonation*.

White Rose Research Online URL for this paper:  
<http://eprints.whiterose.ac.uk/136461/>

Version: Accepted Version

---

**Article:**

Madsen, J., Madden, G., Themistou, E. et al. (2 more authors) (2018) pH-Responsive diblock copolymers with two different fluorescent labels for simultaneous monitoring of micellar self-assembly and degree of protonation. *Polymer Chemistry*, 9 (21). pp. 2964-2976. ISSN 1759-9954

<https://doi.org/10.1039/c8py00111a>

---

**Reuse**

Items deposited in White Rose Research Online are protected by copyright, with all rights reserved unless indicated otherwise. They may be downloaded and/or printed for private study, or other acts as permitted by national copyright laws. The publisher or other rights holders may allow further reproduction and re-use of the full text version. This is indicated by the licence information on the White Rose Research Online record for the item.

**Takedown**

If you consider content in White Rose Research Online to be in breach of UK law, please notify us by emailing [eprints@whiterose.ac.uk](mailto:eprints@whiterose.ac.uk) including the URL of the record and the reason for the withdrawal request.



[eprints@whiterose.ac.uk](mailto:eprints@whiterose.ac.uk)  
<https://eprints.whiterose.ac.uk/>



## pH-responsive diblock copolymers with two different fluorescent labels for simultaneous monitoring of micellar self-assembly and degree of protonation

Received 00th January 20xx,  
Accepted 00th January 20xx

DOI: 10.1039/x0xx00000x

[www.rsc.org/](http://www.rsc.org/)

Jeppe Madsen,<sup>\*a,e</sup> George Madden,<sup>b</sup> Efrosyni Themistou,<sup>c</sup> Nicholas J. Warren<sup>a,d</sup> and Steven P. Armes<sup>\*a</sup>

We report the synthesis of a novel amphiphilic pH-responsive diblock copolymer labeled with two different fluorophores. This copolymer comprises a water-soluble poly(glycerol monomethacrylate) [PGMA] block and a pH-responsive poly(2-(diisopropylamino)ethyl methacrylate) [PDPA] block. Pyrene methacrylate [PyMA] is statistically copolymerized with glycerol monomethacrylate (GMA) to introduce a suitable fluorescent label. The chain-ends of the PDPA block are labelled with cresyl violet perchlorate [CV] by exploiting the spin trap properties of this dye molecule. Below pH 6, fluorescence from both dye labels can be detected, but deprotonation of the PDPA block between pH 6 and 7 leads to strong attenuation of the CV fluorescence owing to formation of a charge transfer complex with the tertiary amine units in the PDPA block. Therefore, changes in the Cresyl Violet fluorescence intensity can be correlated to changes in PDPA protonation. Diblock copolymer self-assembly to form PDPA-core micelles occurs under these conditions, leading to pyrene fluorescence at an excitation wavelength of 405 nm. This allows direct measurement of chain aggregation, whereas using pH-responsive dyes is simply a measure of the degree of protonation. Finally, we show that using CV as a spin trap provides a convenient and versatile route to fluorescently-labeled copolymers prepared by either RAFT or ATRP. Moreover, this cost-effective dye fluoresces in the red part of the visible spectrum at both neutral and acidic pH.

### Introduction

Following Ringsdorf's pioneering work,<sup>1</sup> polymers have been examined as delivery vehicles in nanomedicine for the past four decades.<sup>2–6</sup> In particular, the use of well-defined polymeric assemblies such as micelles and vesicles that are capable of responding to changes in the local environment is of increasing interest, especially in drug delivery.<sup>4,5,7–15</sup> To ensure the safe and precise use of copolymer nanoparticles in drug delivery it is important to be able to not only monitor their spatial distribution *in vitro* and *in vivo*, but also to be able to determine whether such self-assembled nanoparticles actually remain intact, not least because this can determine the release profile of encapsulated drugs. In principle, confocal laser scanning microscopy can provide sensitive, rapid and non-invasive methods for monitoring living organisms.<sup>16,17</sup> Moreover, if appropriate dye labels are utilized, this technique can also be

used to monitor the extent of copolymer aggregation.<sup>18,19</sup> In addition, fluorescent dyes can be used as reporters for a large variety of analytes as well as for probing the local chemical environment.<sup>17,20–26</sup> For example, we recently reported that the dissociation of Nile Blue-labeled pH-responsive poly(2-(methacryloyloxy)ethyl phosphorylcholine)-poly(2-(diisopropylamino)ethyl methacrylate) [PMPC-PDPA] diblock copolymer vesicles can be monitored by comparing emission intensities at selected wavelengths in the far red region of the visible spectrum.<sup>19</sup> The disassembly and the corresponding shift in the fluorescence spectrum is caused by the change in protonation state of the PDPA block and of the dye. The PDPA block has a pKa of around 6.4,<sup>27,28</sup> which is below physiological pH, but above the local pH for (i) cellular compartments such as endosomes<sup>29</sup> and (ii) hypoxic tissue.<sup>30</sup> Since these 'stealthy' vesicles readily enter most types of mammalian cells,<sup>31</sup> they are promising candidates for probing local pH in biological environments.<sup>19</sup> Lowering the pH leads to vesicle dissociation, which causes a corresponding shift in the fluorescence spectrum as a result of partial protonation of the PDPA block. Moreover, such vesicles can be loaded with both hydrophobic and hydrophilic drugs, which are released when the local pH is less than the pKa of the PDPA block.<sup>31,32</sup> Therefore, these dye-labelled vesicles are potential 'self-reporting' drug delivery vehicles. Furthermore, introduction of the Nile Blue was straightforward because this dye reacts directly with propagating polymer radicals, enabling a significant fraction of

*a* Department of Chemistry, University of Sheffield, Brook Hill, Sheffield, S3 7HF, UK  
*b* Science and Technology Facilities Council, Polaris House, Swindon, SN1 1SZ, UK  
*c* School of Chemistry and Chemical Engineering, Queen's University Belfast, Belfast BT9 5AG, UK  
*d* School of Chemical and Process Engineering, University of Leeds, Leeds, LS2 9JT, UK

*e* Danish Polymer Centre, DTU Chemical Engineering, Technical University of Denmark, Søtofts Plads, Bygning 227, rum 118, 2800 Kgs. Lyngby, Denmark

\* Authors of correspondence.

Electronic Supplementary Information (ESI) available: Experimental protocols, details used in the calculation of reactivity ratios and additional characterization of monomers and polymers. See DOI: 10.1039/x0xx00000x

the copolymer chains to be labeled. Despite these very promising results, there are several problems with this prototype system: Firstly, the relative change in fluorescence is related to the degree of protonation of both the PDPA block and the dye label. This parameter can depend on a number of variables, including temperature, ionic strength and the mean degree of polymerization of the PDPA block.<sup>12</sup> In addition, this strategy is not suitable for block copolymers that respond to alternative stimuli. Furthermore, although Nile Blue is cost-effective, the quantum yield for this label is relatively low in aqueous solution.<sup>19,33</sup> This leads to poor sensitivity at low copolymer concentrations or where matrix-associated absorption and/or autofluorescence is prevalent. Finally, the PMPC block is known to rapidly enter all cells that are capable of endocytosis.<sup>32,34</sup> While this is useful for the visualization of intracellular compartments, it is problematic for targeted drug delivery to specific cells. In this case, copolymer vesicles that do not normally enter cells but can be functionalized with appropriate cell receptors are required. In order to address these issues, we have designed second-generation diblock copolymer vesicles. The hydrophilic steric stabilizer block is based on poly(glycerol monomethacrylate) (PGMA), which is readily prepared via reversible addition-fragmentation chain transfer (RAFT) polymerization of glycerol monomethacrylate (GMA). This water-soluble precursor has high chain-end fidelity and has been previously chain-extended by RAFT aqueous dispersion polymerization with 2-hydroxypropyl methacrylate (HPMA) to form well-defined spheres, worms or vesicles.<sup>35,36</sup> Diblock copolymer nano-objects comprising PGMA stabilizer chains do not to enter cells.<sup>35,37</sup> However, if an appropriate targeting group is introduced, highly specific cell uptake can be achieved.<sup>35</sup> For example, GMA can be statistically copolymerized with methacrylic comonomers to introduce desired functional groups into the stabilizer block.<sup>38,39</sup> Alternatively, a binary mixture of a PGMA macro-CTA and a second macro-CTA containing the desired functionality can be used when generating the hydrophobic core-forming block via polymerization-induced self-assembly (PISA).<sup>35,40</sup> In principle, a suitable comonomer, initiator or functional chain transfer agent can also be used to introduce appropriate functionality.<sup>41</sup> Post-polymerization modification of PGMA-based block copolymers is feasible by exploiting the vicinal diol groups in the stabilizer block to form boronate esters<sup>42–45</sup> or acetals/ketals<sup>46,47,48</sup> or by its alcohol group to prepare functional esters.<sup>49</sup> Herein, we show that RAFT statistical copolymerization of GMA with pyrene methacrylate (PyMA)<sup>50</sup> yields water-soluble stabilizer chains containing on average less than one pyrene label per chain that exhibit the characteristic fluorescence of pyrene unimers. Chain extension of such pyrene-labeled stabilizer chains with DPA produces a pH-responsive amphiphilic diblock copolymer, which undergoes self-assembly in aqueous solution at around neutral pH. This leads to an increase in the local pyrene concentration, which causes the formation of pyrene aggregates that fluoresce when excited at 405 nm.<sup>51</sup> In this sense, polymer aggregation leads to changes in the fluorescence spectrum, in contrast to aggregation induced emission (AIE),<sup>52,53</sup> where the emission intensity increases upon

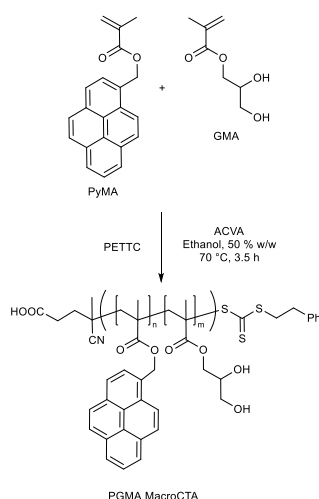
dye aggregation. This emphasises that the underlying mechanism is somewhat different.<sup>54</sup> Moreover, a fluorescent dye with high quantum yield, Cresyl Violet (CV) was conjugated to the ends of the PDPA chains as a probe for chain protonation. When the PDPA chains are deprotonated, the tertiary amines form a charge transfer complex with the dye. This complex has a low quantum yield and an absorption maximum that is shifted towards shorter wavelengths, relative to the free dye.<sup>55</sup> Protonation of the amine leads to disruption of the complex and an increase in fluorescence intensity.

CV is a relatively cheap fluorescent dye with a high quantum yield; it emits in the red region of the visible spectrum and has been used as a histological stain for many years.<sup>56,57</sup> It has been previously utilized as a red dye probe for biological systems. For example, Ma's group modified CV via diazotisation to prepare a ratiometric fluorescent probe for hydrogen sulfide.<sup>58</sup> The same team also prepared an 'on-off' probe based on an oxidised cresyl violet analogue for detection of hypoxia and nitroreductase.<sup>59</sup> These probes were used to examine MCF-7 cells and zebra fish.<sup>58,59</sup> Moreover, CV can react with Vitamin B6 to give a Schiff base derivative that exhibits pH-dependent emission in the visible spectrum.<sup>60</sup>

## Results and discussion

### Synthesis of fluorescently-labelled stabilizer block by RAFT statistical copolymerisation of glycerol monomethacrylate with pyrene methacrylate

The statistical copolymerisation of GMA and PyMA (see Scheme 1) was monitored by <sup>1</sup>H NMR and GPC to examine whether pyrene methacrylate acted as a spin trap, i.e. a compound that reacts with short-lived radicals to form a less reactive adduct. According to the kinetic experiments (see Figure 1A), increasing the proportion of PyMA in this statistical copolymerisation did not have any significant effect on the conversion versus time curve. In addition, the semi-logarithmic plot was approximately linear up to high conversions and did not vary with PyMA concentration, which suggests that the radical concentration is not affected by the presence of PyMA. Furthermore, Figure 1B shows a linear evolution in molecular weight and a gradual reduction in dispersity with conversion. These features are characteristic of a pseudo-living polymerisation and suggest that the PyMA has no detrimental effect on this copolymerisation. It is important to determine to what extent the copolymerization of PyMA and GMA is truly statistical as this may have important consequences for their intended use as aggregation-sensitive probes. For example, if PyMA is incorporated into the copolymer chain significantly faster than GMA, some chains may comprise more than one pyrene units in close vicinity. In principle, this could lead to formation of pyrene aggregates and excimer formation even for molecularly-dissolved chains. The copolymerization was monitored by analyzing a series of aliquots in a kinetics experiments using an HPLC equipped with a diode-array detector. In addition to



Scheme 1: RAFT synthesis of pyrene-labeled PGMA macro-CTA via statistical copolymerization of pyrene methacrylate (PyMA) with glycerol monomethacrylate (GMA) in ethanol at 70 °C

determining the overall comonomer conversion, this HPLC set-up allows simultaneous determination of the relative concentration of each component within the reaction mixture as well as the appearance of any new components, see Figure S1.

In the absence of PyMA, the relative reactivity of the two isomers of GMA (2,3-dihydroxypropyl methacrylate and 1,3-dihydroxypropyl methacrylate<sup>61</sup> can be assessed. According to <sup>1</sup>H NMR analysis, GMA comprises 92 mol % 2,3-dihydroxypropyl methacrylate and 8 mol % 1,3-dihydroxypropyl methacrylate.<sup>36</sup> Plotting the overall conversion (calculated from <sup>1</sup>H NMR) as a function of the comonomer conversion (calculated from HPLC) shows that the minor isomer is copolymerized faster than the major isomer. Applying a non-terminal model to this copolymerization, where the rate of incorporation is governed by the chemical structure of the isomer and not that of the chain-end, reactivity ratios can be calculated based on the available data.<sup>62</sup> These data are provided in Figure S2A. Since both isomers are methacrylates, the corresponding chain-end radicals would be expected to be of comparable reactivity. Nevertheless, the kinetic data indicate that the reactivity ratio of the minor component, 1,3-dihydroxypropyl methacrylate has a reactivity ratio of 1.6, whereas the reactivity ratio of 2,3-dihydroxypropyl methacrylate has a reactivity ratio of 0.7. This would indicate a preference of the minor component to be incorporated faster in the initial stages. However, due to the relatively large excess of the minor component, a near-random copolymer is expected.

Similar observations were made for the copolymerization of GMA with PyMA (see Figure S2 B-D). Strictly speaking, this is a terpolymerization but for simplicity GMA was considered to be a single entity and calculations were performed by combining the signals assigned to its two isomers in the HPLC chromatograms. The data indicate that PyMA is incorporated into the copolymer faster than GMA. Assuming a non-terminal model for GMA, its reactivity ratio is consistently 0.7, which is the same as that found for its major isomer in the absence of

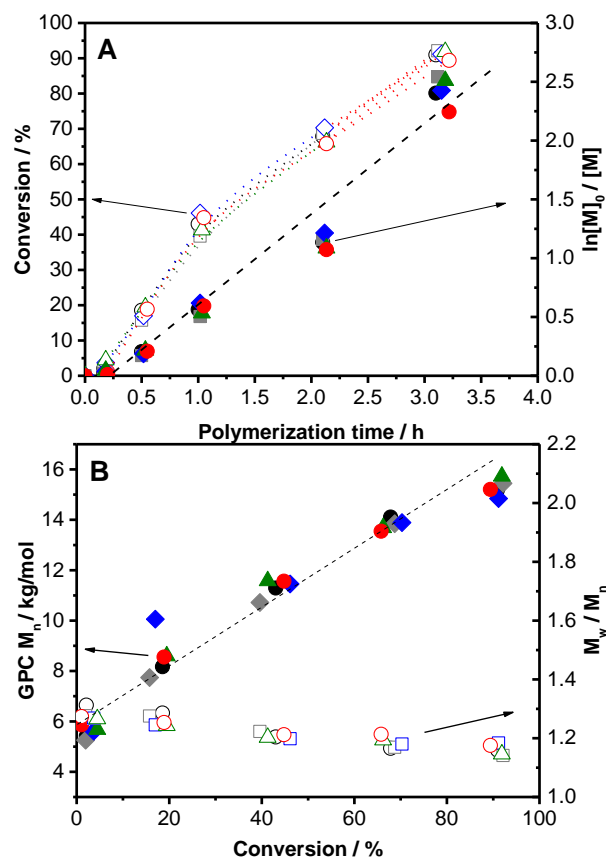


Figure 1: Preparation of PGMA macro-CTA in the presence or absence of pyrene methacrylate comonomer in ethanol at 70 °C. (A) Monomer conversion and semi-logarithmic plot as a function of time. (B) Evolution of  $M_n$  and  $M_w/M_n$  as a function of conversion. Legend: black circles – [PyMA]:[PETTC] = 0. grey squares – [PyMA]:[PETTC] = 0.06. blue squares [PyMA]:[PETTC] = 0.13. green triangles – [PyMA]:[PETTC] = 0.58. red circles – [PyMA]:[PETTC] = 1.1. Conditions: [GMA]:[PETTC]:[ACVA] = 55:1:0.1; [GMA] = 0.0031 mol/g

PyMA (see Figure S2A). In contrast, the reactivity ratio for PyMA lies between 1.2 and 1.6 (see Figures S2B–S2D). This inconsistency suggests that the non-terminal model is not strictly valid. Ideally, reactivity ratios should be determined using a wider range of initial comonomer molar ratios, which is beyond the scope of the current work. Nevertheless, because PyMA is incorporated faster into the copolymer chains than GMA, there is a greater probability of any two pyrene units lying in close proximity (and hence capable of excimer formation). This is particularly likely for the synthesis of macro-CTAs using more than one PyMA per chain in the monomer feed. Thus, 0.54 pyrene units per macro-CTA chain was targeted in this study in order to minimize this potential problem.

#### Absorption and emission of pyrene-labeled PGMA macro-CTAs

Figure 2 shows the absorption and emission spectra obtained for PGMA and P(GMA-co-PyMA) macro-CTAs dissolved in deionised water at room temperature (20 °C). As expected, the former macro-CTA is non-fluorescent and has an absorption band at around 310 nm, which corresponds to its trithiocarbonate end-group (yellow trace).<sup>63,64</sup> The P(GMA-co-

PyMA) macro-CTA has additional features at 268 nm, 274 nm, 318 nm, 330 nm and 346 nm, which are assigned to the fine structure expected for pyrene.<sup>50,65</sup> Moreover, fluorescence bands corresponding to the pyrene units<sup>66,67</sup> are observed between 350 nm and 450 nm at an excitation wavelength of 342 nm.<sup>50</sup> The weak emission intensity above 450 nm suggests little excimer formation,<sup>66,67</sup> as expected for near molecularly-dissolved copolymer chains containing less than one dye label per chain. The fluorescence intensity of an aqueous solution of P(GMA-co-PyMA) containing approximately one PyMA unit per chain might be expected to be around twice that of a P(GMA-co-PyMA) containing 0.54 PyMA units per chain. However, as Figure 2 clearly shows, the fluorescence intensity of the former copolymer is only slightly higher than that of the latter. The former copolymer also exhibits a broad, albeit weak, fluorescence signal above 450 nm. This suggests some excimer formation arising from the larger amount of pyrene units per copolymer chain. In view of these observations, the P(GMA-co-PyMA) macro-CTA containing 0.54 PyMA units per chain was selected to minimize *intra*-chain pyrene-pyrene interactions for the doubly-labeled diblock copolymers targeted in this study.

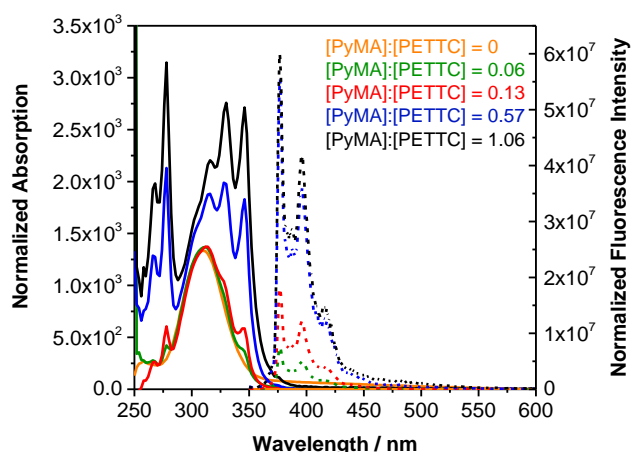


Figure 2: Absorption and emission recorded for P(GMA-co-PyMA) macro-CTAs containing an increasing proportion of pyrene methacrylate comonomer. All spectra were recorded in deionized water and normalized with respect to the copolymer concentration. Excitation wavelength = 342 nm.

#### Preparation of doubly-labeled PGMA-PDPA diblock copolymers

Next, a P(GMA<sub>61</sub>-co-PyMA<sub>0.54</sub>) macro-CTA was chain-extended with DPA to prepare a (PGMA-co-PyMA)-PDPA diblock copolymer according to Scheme 2A. In addition, the effect of adding cresyl violet (CV; in its perchlorate salt form) to the DPA polymerization was investigated, as shown in Scheme 2B.

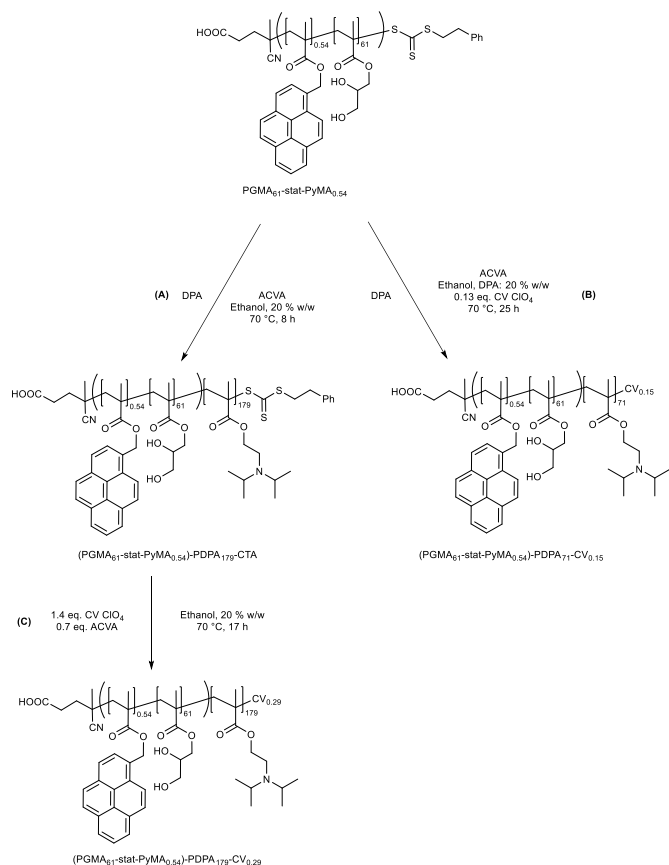
Figure 3 shows the DPA conversion vs. time curve and the corresponding semi-logarithmic plot. In the absence of CV, the DPA polymerization proceeds to around 70 % conversion within 8 h at 70 °C. However, the semi-logarithmic plot is only linear up to around 40 % conversion, which suggests imperfect control over this polymerization. This is consistent with the relatively broad molecular weight distributions ( $M_w/M_n \sim 1.5$ -1.6)

obtained for the final diblock copolymers (see Table 1). Significantly lower polydispersities ( $M_w/M_n \sim 1.3$ -1.4) have been reported for the synthesis of other PDPA-containing block copolymers by RAFT polymerization.<sup>28,68,69</sup> For the PGMA-PDPA diblock copolymers described herein, it proved difficult to identify a suitable common solvent; ethanol dissolves PGMA and PDPA homopolymers as well as DPA monomer, but addition of the DPA monomer to an ethanolic solution of PGMA led to the formation of a white suspension. The suspension did not disappear simply upon heating. However, a transparent solution was obtained within 15-30 min during polymerisation, i.e. in the presence of radical initiator. Such a delay corresponds to a DPA conversion of 5-10 % according to the kinetic data shown in Figure 3. In principle, this inhomogeneity could lead to the formation of PDPA homopolymer by a free radical mechanism, which may in part explain the broadening of the molecular weight distribution. In addition, chain transfer to the isopropyl groups on DPA/PDPA may occur in such syntheses.<sup>70</sup> Clearly, it is desirable to identify a more suitable solvent for the RAFT polymerization of DPA. Nevertheless, as a proof-of-concept study to demonstrate the use of doubly-labeled diblock copolymer probes the relatively high polydispersity is not a serious drawback.

Based on our previous work with Nile Blue derivatives,<sup>19</sup> we hypothesized that cresyl violet (CV) should act as a spin trap given its similar chemical structure to the former dye. Based on the literature for structurally related dyes such as methylene blue<sup>71</sup> and phenothiazine,<sup>72</sup> the radical-dye reaction is likely to follow the pathway outlined in Scheme S1. The propagating polymer radical initially undergoes chain transfer to CV, which produces a terminated chain and a dye radical. The latter species is stabilized and therefore does not readily initiate new polymer chains.<sup>71</sup> However, this dye radical can react with a second polymer radical to form a non-propagating dye-labeled chain. As every chain-labeling event consumes two propagating radicals, the maximum fraction of labeled chains is 0.50, provided that the CV is present in sufficient excess. However, using excess dye leads to more effective radical quenching which suppresses the polymerization.

In the presence of 0.13 equivalent CV per chain, the DPA polymerisation only proceeds to around 25 % conversion (see Figure 3A). The semi-logarithmic plot (Figure 3B) deviates significantly from linearity, which indicates consumption of polymer radicals via reaction with CV, which acts as a spin trap under such conditions. Visible absorption spectroscopy studies indicated that every CV is attached to a chain (see Table 1, entry 1).

The effect of adding CV and ACVA (CV:ACVA:CTA molar ratio = 1.40:0.70:1.00) as a degassed solution in ethanol to DPA polymerizations at around 70 % DPA conversion was investigated (see Scheme 2C). Under such conditions, approximately 30 % of the copolymer chains can be labeled with CV (see Table 1, entry 2). Since the radicals are generated by the ACVA initiator, increasing its concentration might lead to a higher proportion of CV-labeled chains. However, a higher



Scheme 2: Synthetic routes to doubly-labeled (PGMA<sub>61</sub>-co-PyMA<sub>0.54</sub>)-PDPA-CV<sub>x</sub> diblock copolymers by termination with cresyl violet (CV): (A) RAFT polymerization in the absence of CV; (B) Chain extension of a PGMA<sub>61</sub>-co-PyMA<sub>0.54</sub> macro-CTA by RAFT polymerization of DPA in the presence of CV; (C) Labeling of (PGMA<sub>61</sub>-co-PyMA<sub>0.54</sub>)-PDPA diblock

radical concentration may also increase the probability of CTA removal.<sup>74,75</sup> In principle, it may be feasible to optimize the degree of labeling by systematic variation of the relative amounts of CV and ACVA, but this possibility has not been explored further here. Nevertheless, given the relatively high quantum yield of cresyl violet of around 0.50,<sup>56,47</sup> 30 % chain labeling should allow fluorescence tracking of such copolymers in cells and/or tissue. For example, Nile Blue-labeled copolymers could be visualized within cells and multicellular tumor models, despite quantum yields of around 0.10 and achieving only 10-15 % chain functionalization.<sup>19</sup>

The synthesis of CV-labeled polymers was also investigated using atom transfer radical polymerization (ATRP). Figure S3 shows the ATRP kinetics for a 2-(methacryloyloxy)ethyl phosphorylcholine (MPC) monomer in the absence and presence of CV. Increasing the concentration of this dye label leads to retarded polymerizations and hence lower overall monomer conversions. Inspecting the data presented in Table S1 confirms that, while approximately half of the copolymer chains can be labeled with CV by adding one equivalent of this dye per initiator primary radical, such conditions lead to a lower overall conversion and thereby a reduced degree of polymerization. In addition, this approach leads to a significant

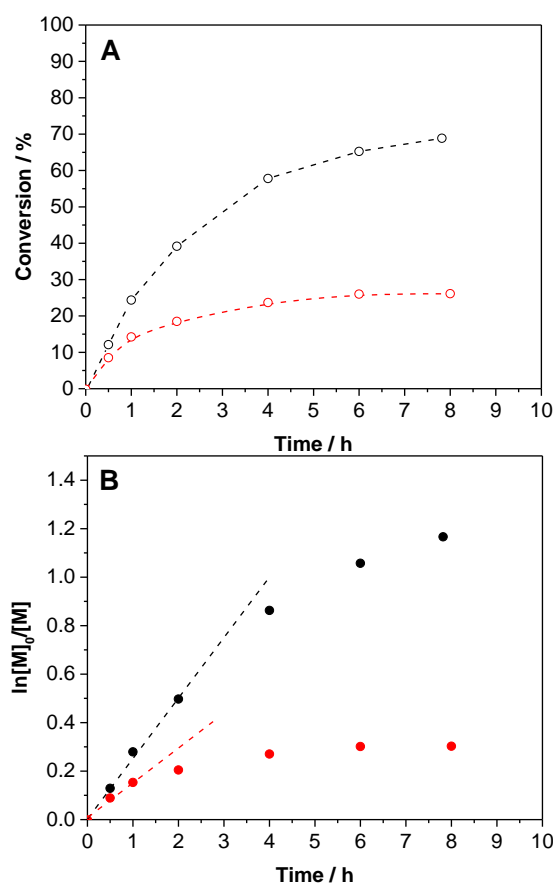


Figure 3: Preparation of a (PGMA-co-PyMA)-PDPA diblock copolymer from (PGMA-co-PyMA) macro-CTA by RAFT polymerisation of DPA at 70 °C in the absence or presence of CV ClO<sub>4</sub>: (A) Conversion versus time curve and (B) corresponding semi-logarithmic plot. Conditions: [DPA]:[P(GMA<sub>61</sub>-co-PyMA<sub>0.55</sub>)]:[ACVA] molar ratio= 240:1.00:0.50. [P(GMA<sub>61</sub>-co-PyMA<sub>0.55</sub>)] = 17.3 mol/kg

amount of free dye remaining in the reaction solution. On the other hand, adding 0.50 equivalents of CV leads to an overall DPA conversion of 80 % with 22 % CV-labeled chains. Thus, CV acts as a less efficient radical quencher in such ATRP syntheses compared to the RAFT polymerisation syntheses described above. However, this observation is at least as likely to be the result of differences in monomer type, reaction temperature and concentration, as any intrinsic differences between ATRP and RAFT polymerization chemistries.

Table 1: Characterization of target P(GMA<sub>61</sub>-co-PyMA<sub>0.54</sub>)-PDPA<sub>240</sub> diblock copolymers where CV is either present throughout the polymerization or added at 70 % conversion

Entry	CVCIO <sub>4</sub> dye addition details	NMR composition <sup>a</sup>	Composition after purification <sup>b</sup>	Maximum conversion	M <sub>n</sub> <sup>c</sup>	M <sub>w</sub> /M <sub>n</sub> <sup>c</sup>	CV per copolymer chain <sup>d</sup>
1	0.13 equivalent CV ClO <sub>4</sub> present throughout	(PGMA <sub>61</sub> -co-PyMA <sub>0.54</sub> )-PDPA <sub>71</sub>	(PGMA <sub>61</sub> -co-PyMA <sub>0.54</sub> )-PDPA <sub>64</sub>	30 %	15 900	1.49	0.15 ± 0.01
2	1.4 equivalent CV ClO <sub>4</sub> and 0.7 equivalent ACVA added at 70 % conversion	(PGMA <sub>61</sub> -co-PyMA <sub>0.54</sub> )-PDPA <sub>179</sub>	(PGMA <sub>61</sub> -co-PyMA <sub>0.54</sub> )-PDPA <sub>202</sub>	74 %	25 700	1.63	0.29 ± 0.02

<sup>a</sup> Copolymer composition based on the monomer/CTA molar ratio multiplied by the DPA conversion calculated using <sup>1</sup>H NMR spectroscopy. <sup>b</sup> Copolymer composition based on relative <sup>1</sup>H NMR signals for the GMA and DPA residues after dialysis against ethanol, methanol and water. <sup>c</sup> THF GPC after derivatization of GMA residues using excess benzoic anhydride in pyridine. <sup>d</sup> Cresyl violet content calculated using an integrated absorbance coefficient for cresyl violet perchlorate determined in 0.10 M HCl<sup>73</sup>

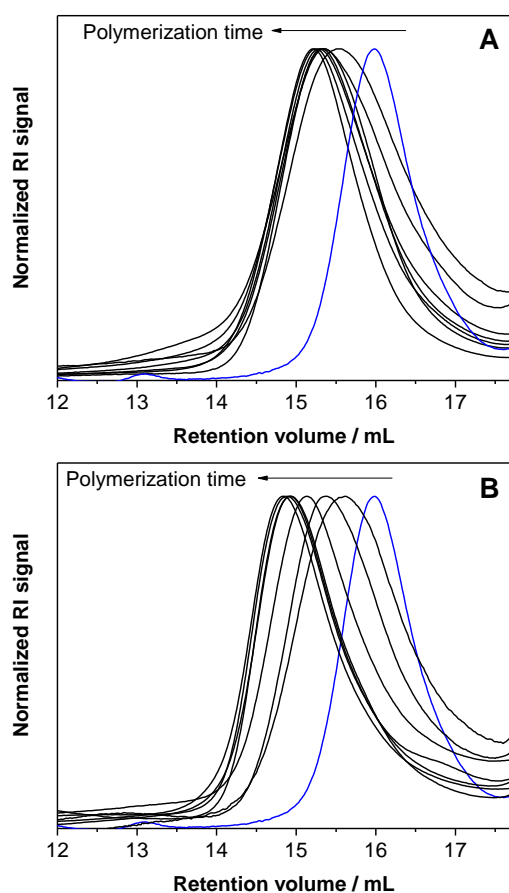


Figure 4: THF GPC curves obtained for P(GMA-co-PyMA)-PDPA block copolymers during kinetics studies after derivatization of the hydroxy groups of the GMA residues using excess benzoic anhydride in pyridine. (A) GPC curves for P(GMA-co-PyMA)-PDPA prepared in the absence of any CV. (B) GPC curves for P(GMA-co-PyMA)-PDPA obtained in the presence of 0.13 equivalents of CV ClO<sub>4</sub>. The arrow indicates increasing conversion. Conditions: [DPA]:[P(GMA<sub>61</sub>-co-PyMA<sub>0.55</sub>)]:[ACVA] = 240:1.00:0.50. [P(GMA<sub>61</sub>-co-PyMA<sub>0.55</sub>)] = 17.3 mol/kg, 70 °C.

#### Absorption and emission of doubly-labeled PGMA-PDPA diblock copolymers

Figure 5 shows uv-visible absorption spectra recorded for the two different doubly-labeled P(GMA-co-PyMA)-PDPA-CVx

diblock copolymers dissolved in either ethanol or 0.1 M aqueous HCl, as well as the reference spectrum of cresyl violet perchlorate dissolved in 0.1 M aqueous HCl. The PDPA block is molecularly dissolved in aqueous HCl (Figure 5, red traces). Below 360 nm, a distinctive absorption envelope is observed that is assigned to the copolymerized pyrene methacrylate units in the P(GMA-co-PyMA) block. The CV label absorbs from 500 nm to 700 nm. Notably, its absorption maximum in aqueous HCl is red-shifted from 590 nm for the free dye to approximately 615 nm when incorporated as a terminal group on the copolymer chains (see Figure 5 and Table 2). This is attributed to an inductive, electron-donating substituent on one (or both) of the amine groups.<sup>76</sup> Amine substitution is a well-known reaction between radicals and aromatic amines.<sup>72,77</sup> Therefore, this red-shifted absorption provides spectroscopic evidence for CV conjugation to the copolymer chain-ends.

Ethanol dissolves the copolymer chains, albeit with the PDPA block in its neutral (unprotonated) form. However, the pyrene absorption spectrum for such copolymer solutions is only marginally different, presumably due to changes in solvent polarity.<sup>65</sup> In contrast, the cresyl violet absorption maximum shifted from 615 nm in 0.1 M aqueous HCl to less than 490 nm in ethanol. The latter wavelength corresponds to the absorption band assigned to the charge transfer complex formed between cresyl violet and aliphatic amines.<sup>55</sup> In this particular case, the neutral PDPA chain constitutes the aliphatic amine.

Figure 6 shows the emission spectra recorded for P(GMA<sub>61</sub>-co-PyMA<sub>0.55</sub>)-PDPA<sub>202</sub>-CV<sub>0.29</sub> dissolved in ethanol (Figure 6A) and in 0.1 M aqueous HCl (Figure 6B) when excited at 342 nm, 405 nm, 488 nm and 543 nm. The corresponding spectra obtained for cresyl violet perchlorate in 0.1 M aqueous HCl is also shown as a reference (Figure 6C). The dotted lines are the corresponding absorption spectra recorded in the same solvents. An excitation wavelength of 342 nm is commonly used for pyrene,<sup>50</sup> and the other three wavelengths are laser wavelengths that are typically used in confocal laser scanning microscopy. Pyrene excimer species absorb at 405 nm and fluoresce when excited at this wavelength.<sup>51</sup> The cresyl violet-amine charge transfer complex absorbs at 488 nm, while cresyl violet absorbs at 543 nm.<sup>55</sup> Hence the emission spectra observed when using these excitation wavelengths can be used to assess the degree of protonation of the PDPA block (*vide infra*).

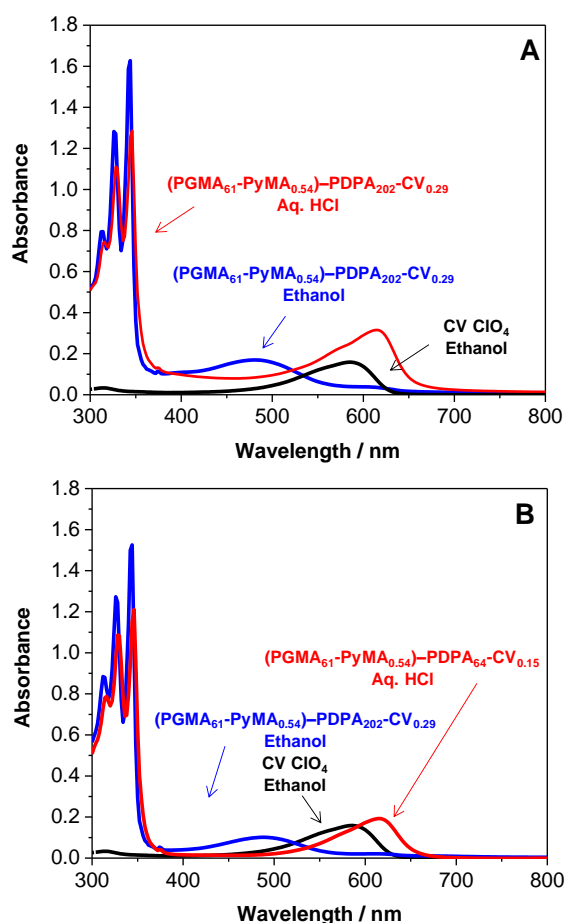


Figure 5: UV-visible absorption spectra recorded for P(GMA-co-PyMA)-PDPA-CV diblock copolymers in either ethanol or aqueous 0.1 M HCl. A reference spectrum for CV ClO<sub>4</sub> in 0.1 M HCl is included for comparison. (A) [P(GMA<sub>61</sub>-co-PyMA<sub>0.54</sub>)-co-PDPA<sub>202</sub>-CV<sub>0.29</sub>] = 3.12 g/L. (B) [P(GMA<sub>61</sub>-co-PyMA<sub>0.54</sub>)-PDPA<sub>64</sub>-CV<sub>0.15</sub>] = 1.35 g/L. [CV ClO<sub>4</sub>] = 0.0036 g/L.

Subjecting the copolymer solutions to an excitation wavelength of 342 nm leads to the well-known emission spectrum for pyrene both in ethanol and in 0.1 M HCl (see Figure 6A and 6B, respectively). Weak fluorescence is observed at 623 nm in the solution of P(GMA<sub>61</sub>-co-PyMA<sub>0.55</sub>)-PDPA<sub>202</sub>-CV<sub>0.29</sub> in 0.1 M aqueous HCl and also in the spectrum obtained for cresyl violet (see Figure 6C); this simply reflects the very low absorbance of cresyl violet at 342 nm (N.B. The 684 nm signal is an instrument artefact corresponding to double the excitation wavelength). Excitation of the ethanol solution at 405 nm (Figure 6A) gives an emission signal at around 500 nm. This corresponds to the formation of pyrene excimers,<sup>51</sup> which indicates that the copolymer chains are aggregated to some extent in ethanol. However, this aggregation is weak, as indicated by the ratio between the pyrene monomer and excimer emission intensity observed at an excitation wavelength of 342 nm. This suggests that excitation at 405 nm must be highly sensitive to pyrene aggregation. Use of the latter wavelength does not allow pyrene to be used as a 'molecular ruler', as reported for the shorter excitation wavelength, because the unimers are not excited.<sup>50</sup>

The emission spectrum recorded for the ethanolic copolymer solution excited at 405 nm has a shoulder above 600 nm (Figure 6A), which suggests simultaneous excitation of the cresyl violet label. On the other hand, essentially no pyrene signal is observed in 0.1 M aqueous HCl, where a cresyl violet feature centred at 635 nm dominates the emission spectrum (see Figure 6B). This is consistent with no copolymer aggregation occurring at low pH because the protonated PDPA blocks are highly cationic and hence hydrophilic. The corresponding signal for cresyl violet is observed at 625 nm (Figure 6C). The bathochromic shift observed for the copolymer emphasizes the differing spectral properties of this chromophore when conjugated to the copolymer chains, as discussed above.

Excitation of a solution of P(GMA<sub>61</sub>-co-PyMA<sub>0.55</sub>)-PDPA<sub>202</sub>-CV<sub>0.29</sub> at 488 nm leads to broad emission bands, with maxima at 599 nm in ethanol and 619 nm in 0.1 M aqueous HCl (see Figure 6A and 6B, respectively, and Table 2). In contrast, CV ClO<sub>4</sub> exhibits a maximum emission at 625 nm in 0.1 M aqueous HCl. In addition, the free dye has a secondary band at 570 nm (see Figure 6C). To the best of our knowledge, this local maximum has not been previously described for cresyl violet. Presumably, this is because most studies of its fluorescence tend to use longer excitation wavelengths, which would suppress this feature. This is illustrated by comparison with the fluorescence spectrum obtained for the free dye in Figure 6C recorded using an excitation wavelength of 543 nm. In this latter spectrum, the 570 nm band is reduced to a weak shoulder. A rigorous explanation of this additional spectral feature is beyond the scope of the current work, but we note that at least some commercial batches of cresyl violet can apparently contain significant amounts of 9-amino-benzo[α]phenoxazin-5-one.<sup>57</sup> This dye is denoted cresyl red (CR) by analogy with the structurally similar Nile Red (NR) and Nile Blue (NB).<sup>78</sup> To the best of our knowledge, the full photochemical characterization of CR has not been reported. However, it absorbs at significantly shorter wavelengths than CV in protic solvents, exhibiting hypsochromic shifts of around 80-90 nm.<sup>57</sup> Despite this relatively large difference, the absorption spectra of mixtures of CV and CR comprising 40-50 % CR were reported to be almost indistinguishable from a spectrum obtained for pure CV.<sup>57</sup> The hypsochromic shift in the absorption spectrum between CV and CR correlates well with those observed for Nile Blue and Nile Red.<sup>78</sup> Thus, provided that the fluorescence follows a similar pattern as that observed for the latter dye pair, contamination with CR may account for the unexpected shoulder observed at 570 nm noted above.

Excitation at 543 nm leads to emission maxima at 635 nm in 0.1 M aqueous HCl (Figure 6B and Table 2) and at 620 nm in ethanol (Figure 6A and Table 2) for P(GMA<sub>61</sub>-co-PyMA<sub>0.55</sub>)-PDPA<sub>202</sub>-CV<sub>0.29</sub>. In both cases the intensity is higher than for the spectra obtained using an excitation wavelength of 488 nm (see Figure 6). This mainly reflects the difference in absorption of the non-complexed dye at these two wavelengths (see Figure 5). In both cases, the maxima are more red-shifted than for the same solutions excited at 488 nm. If this batch of cresyl violet does indeed contain some cresyl red impurity (vide supra), and assuming that this second dye label is also incorporated into the

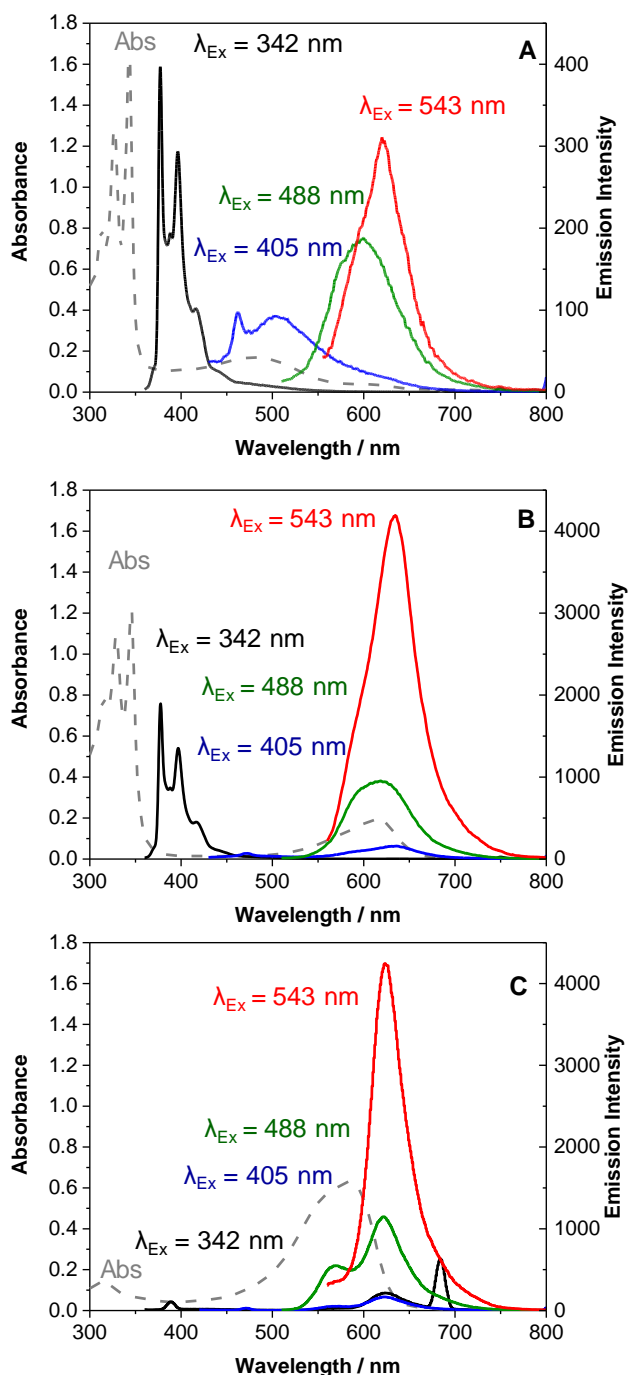


Figure 6: Emission spectra recorded for P(GMA<sub>61</sub>-co-PyMA<sub>0.55</sub>)-PDPA<sub>202</sub>-CV<sub>0.29</sub> and CV ClO<sub>4</sub> using relevant laser wavelengths (dotted lines show absorption spectra). (A) P(GMA<sub>61</sub>-co-PyMA<sub>0.55</sub>)-PDPA<sub>202</sub>-CV<sub>0.29</sub> dissolved in ethanol. (B) P(GMA<sub>61</sub>-co-PyMA<sub>0.55</sub>)-PDPA<sub>202</sub>-CV<sub>0.29</sub> dissolved in 0.1 M aqueous HCl. (C) CV ClO<sub>4</sub> dissolved in 0.1 M aqueous HCl. For spectra recorded using an excitation wavelength of 342 nm, excitation and emission slits were both set to 2.5 nm. For all other spectra, excitation and emission slits were both set to 5 nm so as to compare relative intensities between wavelengths and solvents. Fluorescence spectra concentrations: [P(GMA<sub>61</sub>-co-PyMA<sub>0.55</sub>)-PDPA<sub>202</sub>-CV<sub>0.29</sub>] = 0.312 g/L. [CV ClO<sub>4</sub>] = 0.536 • 10<sup>-3</sup> g/L. Absorption spectra concentrations: [P(GMA<sub>61</sub>-co-PyMA<sub>0.55</sub>)-PDPA<sub>202</sub>-CV<sub>0.29</sub>] = 3.12 g/L. [P(GMA<sub>61</sub>-co-PyMA<sub>0.55</sub>)-PDPA<sub>64</sub>-CV<sub>0.15</sub>] = 1.35 g/L. [CV ClO<sub>4</sub>] = 0.0036 g/L.

copolymer chains to some extent, then this difference can be explained by the preferential absorption of cresyl violet at 543 nm (since it has maximum emission at longer wavelengths).

It is possible to directly compare emission intensities in Figure 6 because identical spectrophotometer settings were used and the copolymer concentration in ethanol and 0.1 M aqueous HCl was the same within experimental error. For the latter copolymer solution, the ratio of maximum emission intensities of the cresyl violet part of the spectrum when excited at 488 nm and 543 nm, respectively, is smaller than that determined in ethanol (see Figure 6). This is illustrated in Table 2, where the ratio of the fluorescence emission observed for P(GMA<sub>61</sub>-co-PyMA<sub>0.54</sub>)-PDPA<sub>202</sub>-CV<sub>0.29</sub> solutions excited at 488 nm compared to that at 543 nm is reduced from 0.60 in ethanol to 0.23 in 0.1 M aqueous HCl. These results suggest that the degree of protonation of the PDPA chains can be monitored by determining the fluorescence intensity ratios recorded using excitation wavelengths of 488 nm and 543 nm. Such ratiometric measurements are attractive because they do not depend on absolute intensities.

The quantum yields observed for the copolymers in ethanol are almost an order of magnitude lower than that obtained in 0.1 M aqueous HCl (see Table 2). Even if the typical error on such measurements exceeds 10 %, <sup>79</sup> this still constitutes a significant difference. The relatively low quantum yields for the copolymers in ethanolic solution are mainly the result of charge transfer complexes being formed between the tertiary amine groups and cresyl violet.<sup>55</sup> On the other hand, the quantum yields observed for the copolymers dissolved in 0.1 M aqueous HCl are significantly higher than the reported reference value of 0.44 for free cresyl violet in water.<sup>80</sup> Presumably, the sterically-hindered copolymer chains suppress the formation of non-fluorescent H-dimers relative to the free dye label.<sup>81</sup> This effect is also observed for cresyl violet-labeled PMPC homopolymers prepared by ATRP, which exhibit quantum yields of 0.60-0.70 (see Table S1).

#### Aggregation of doubly-labeled diblock copolymers

Since PDPA is highly hydrophobic in its deprotonated form,<sup>82</sup> increasing the pH of an aqueous solution of P(GMA-co-PyMA)-PDPA-CV above the pK<sub>a</sub> of PDPA is expected to lead to micellar self-assembly. Since the P(GMA-co-PyMA) block remains water-soluble regardless of the solution pH, it acts as the steric stabiliser for the self-assembled nanoparticles. Other PDPA-based diblock copolymers comprising poly(ethylene glycol) [PEO],<sup>83</sup> poly(2-hydroxypropyl methacrylamide)<sup>68</sup> or PMPC stabilizer blocks<sup>84-86</sup> can form spherical micelles, worm-like micelles or vesicles in aqueous solution depending on the relative degrees of polymerization of the hydrophilic and hydrophobic blocks, as dictated by the packing parameter principle introduced by Israelachvili and co-workers.<sup>87</sup>

Table 2: Photophysical characterization of P(GMA-co-PyMA)-PDPA-CV dissolved in either ethanol or 0.1 M aqueous HCl

Copolymer	Solvent	$\lambda_{\max}$ Abs <sup>a</sup>	$\lambda_{\max}$ E <sub>m</sub> ( $\lambda_{\text{ex}} = 488$ nm) / nm <sup>b</sup>	$\lambda_{\max}$ E <sub>m</sub> ( $\lambda_{\text{ex}} = 543$ nm) / nm <sup>b</sup>	488/543 maximum emission ratio / nm <sup>c</sup>	$\Phi$ ( $\lambda_{\text{ex}} =$ 488 nm) <sup>d</sup>	$\Phi$ ( $\lambda_{\text{ex}} = 543$ nm) <sup>d</sup>
P(GMA <sub>61</sub> -co-PyMA <sub>0.54</sub> )-PDPA <sub>202</sub> -CV <sub>0.29</sub>	Aqueous HCl	614	635	635	0.23	0.51	1.00
P(GMA <sub>61</sub> -co-PyMA <sub>0.54</sub> )-PDPA <sub>202</sub> -CV <sub>0.29</sub>	Ethanol	480	599	620	0.60	0.06	0.15
P(GMA <sub>61</sub> -co-PyMA <sub>0.54</sub> )-PDPA <sub>64</sub> -CV <sub>0.15</sub>	Aqueous HCl	616	636	636	0.15	0.69	0.93
P(GMA <sub>61</sub> -co-PyMA <sub>0.54</sub> )-PDPA <sub>64</sub> -CV <sub>0.15</sub>	Ethanol	489	584	622	0.83	0.06	0.12

<sup>a</sup> Maximum absorption wavelength for cresyl violet chromophore (between 400 nm and 800 nm)

<sup>b</sup> Maximum emission wavelength for cresyl violet fluorophore (between 500 nm and 800 nm)

<sup>c</sup> Ratio between non-normalized maximum emission intensities of solutions excited at 488 nm and 543 nm respectively, with spectrometer settings: Excitation and emission slit: 5 nm. PMT voltage: 950 V

<sup>d</sup> Relative quantum yield calculated according to reference.<sup>79</sup> According to this reference, the error using this method can be anticipated to be (significantly) more than 10%. cresyl violet dissolved in 0.1 M HCl was used as a reference fluorophore. The reference value of the quantum yield of cresyl violet used was 0.44.80

Increasing the pH of a 0.13 g/L aqueous solution of P(GMA<sub>61</sub>-co-PyMA<sub>0.55</sub>)-PDPA<sub>64</sub>-CV<sub>0.15</sub> from pH 3 to pH 7.2 leads to the formation of a turbid solution. Figure 7A shows the dynamic light scattering results obtained using cumulants analysis, which indicates the formation of colloidal aggregates ranging in size between 100 nm and 1000 nm. Confocal laser scanning microscopy (CLSM) images of the copolymer solution excited using a 405 nm laser (Figure 7B) at pH 3 shows a uniform fluorescent signal, corresponding to molecularly-dissolved copolymer chains. In contrast, images recorded at pH 7.2 indicate discrete aggregates with significantly higher fluorescence intensity. This observation is consistent with the formation of relatively large aggregates indicated by dynamic light scattering (Figure 7A).

The fluorescence spectra for the copolymer solutions excited at 405 nm at pH 3 and pH 7.2 could be obtained using the capability of the microscope of acquiring spectral information of the emitted light. These spectra are shown in Figure 7C. At pH 3, a feature at approximately 630 nm dominates the spectrum; this is assigned to the fluorescence of a cresyl violet label conjugated to the copolymer chains (compare to Figure 6B). At pH 7.2, there is an apparent hypsochromic shift of 10 nm for this emission feature. However, since images were recorded for every 10 nm, and the band width was set to 10 nm, this corresponds to a maximum shift. In addition, a new broad signal between 440 nm and 570 nm appears for a copolymer solution in ethanol, which indicates the formation of pyrene aggregates (see Figure 6A). The emission spectra are complicated by the

reflective properties of the glass slides. This leads to 'dips' (at ~510 nm for the pH 7.2 spectrum) that are the result of destructive interference between direct fluorophore emission and the associated reflected emission.<sup>88</sup> Nevertheless, these spectra indicate the formation of pyrene excimer species as a result of copolymer aggregation, as expected. Thus, these doubly-labeled copolymers can be visualized via their cresyl violet chromophore while simultaneously examining their degree of aggregation using their pyrene labels. The effect of changing the solution pH is demonstrated in Figure 7D, where excess gluconolactone is added to a copolymer solution at zero time ( $t = 0$ ). Slow hydrolysis of gluconolactone over time leads to a gradual reduction in solution pH, which eventually leads to dissolution of the initial copolymer aggregates.

The time dependence of the ratio in fluorescence intensity between 500 nm and 550 nm (corresponding to pyrene excimer fluorescence) and also between 600 nm and 700 nm (corresponding to cresyl violet fluorescence) is shown in Figure 7D. Dissociation of the copolymer aggregates leads to disappearance of the excimer signal between 500 nm and 550 nm. At the same time, protonation of the PDPA chains causes a reduction in amine quenching of the cresyl violet fluorescence, leading to an increase in fluorescence between 600 nm and 700 nm. The inset fluorescence microscopy images indicate an overall reduction in fluorescence intensity over time. It is noteworthy that the reduction in the solution pH in the presence of gluconolactone occurs significantly faster than the 17.5 min time scale for this experiment (see Figure S4).

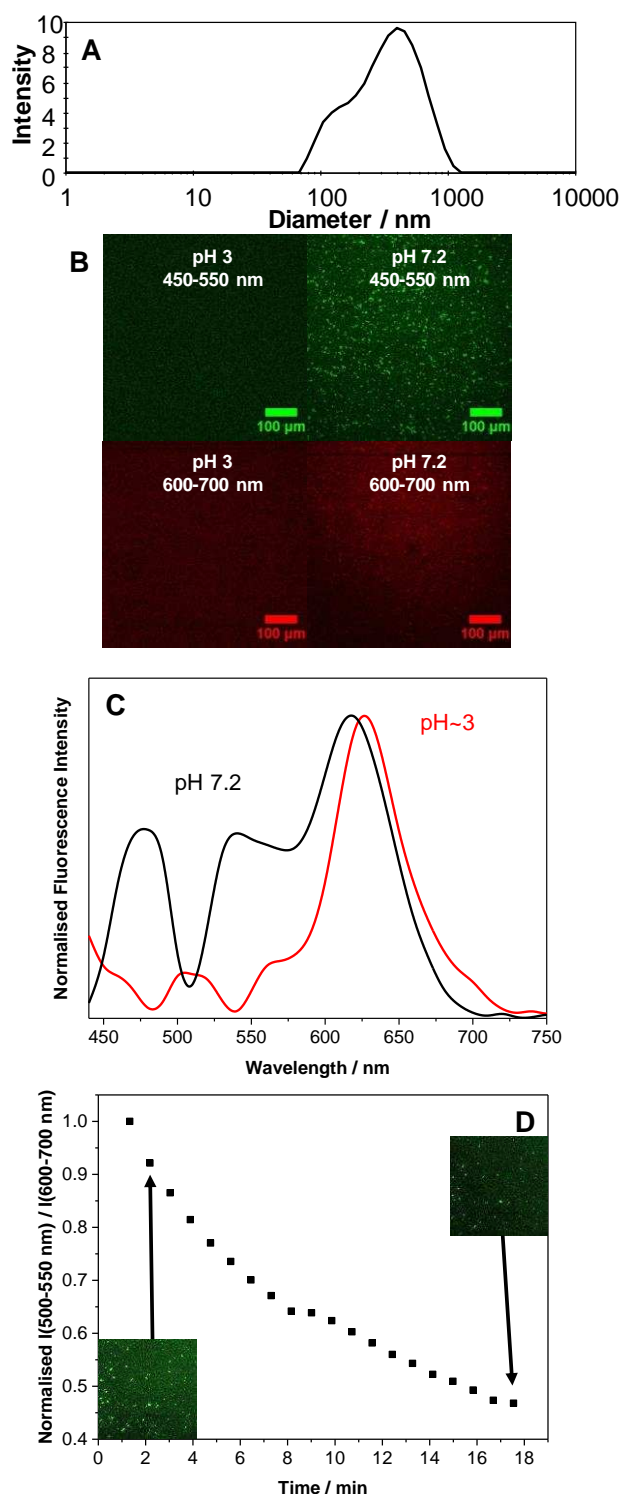


Figure 7: Particle characterization and effect of pH. (A) Intensity-average light scattering intensity versus diameter for a solution of 0.13 g/L P(GMA<sub>61</sub>-co-PyMA<sub>0.55</sub>)-PDPA<sub>64</sub>-CV<sub>0.15</sub> in 0.1 M aqueous HCl at pH 7.2 (after increasing from pH 3 using 1 M NaOH) prior to addition of gluconolactone. (B) CLSM images obtained for P(GMA<sub>61</sub>-co-PyMA<sub>0.55</sub>)-PDPA<sub>64</sub>-CV<sub>0.15</sub> excited using a 405 nm laser at pH 3 and pH 7.2. Green: 450-550 nm. Red: 600-700 nm. (C) Spectra obtained using a CLSM capable of recording spectral information for the emitted light of a 1.1 g/L solution of P(GMA<sub>61</sub>-co-PyMA<sub>0.55</sub>)-PDPA<sub>64</sub>-CV<sub>0.15</sub> in 0.1 M aqueous HCl (pH 3, red) and of the same solution at pH 7.2 (black). (D) Fluorescence intensity ratios determined from CLSM images recorded from 500 to 550 nm and from 600 to 700 nm as a function of time after addition of 0.06 M gluconolactone at 20 °C. Insets: CLSM images recorded for the 500-550 nm interval at the stated time points.

However, there is a self-buffering effect owing to the basicity of the PDPA chains. The resolution of the microscope is not sufficient to resolve aggregates smaller than 1-2  $\mu\text{m}$ , but the overall fluorescence at 500-550 nm is reduced as these aggregates gradually dissociate.

## Conclusions

In summary, doubly-labeled amphiphilic pH-responsive diblock copolymers can be prepared by incorporating pyrene methacrylate into the hydrophilic stabilizer block and terminating the hydrophobic block using cresyl violet as a chain transfer agent. Copolymer aggregation leads to a characteristic change in the absorption and emission characteristics of the pyrene label. Combined with the ability of cresyl violet to form non-fluorescent complexes with tertiary amines, this strategy enables simultaneous monitoring of both the extent of copolymer aggregation and the degree of protonation of the pH-responsive hydrophobic block.

In principle, the general strategy outlined here should have broader scope for a range of applications. The emission fluorescence of pyrene aggregates excited at 405 nm should allow monitoring of the extent of copolymer aggregation in living cells using confocal laser scanning microscopy. This excitation wavelength should be well-tolerated living cells, unlike the UV wavelengths normally required to monitor pyrene aggregation. In addition, labeling copolymers with cresyl violet should be applicable to many, if not all, types of radical polymerization chemistries. The relatively strong absorption and high quantum yield of a cost-effective dye label such as cresyl violet combined with its emission in the red region of the visible spectrum makes this an attractive protocol for monitoring the fate of copolymer nanoparticles in cells and/or tissue.

## Conflicts of interest

The authors declare no competing financial interest.

## Acknowledgements

The authors are grateful to EPSRC (Programme Grant EP/I012060/1 and equipment grant EP/M028437/1) for Financial Support.

## References

- H. Ringsdorf, *J. Polym. Sci. Polym. Symp.*, 1975, **51**, 135–153
- T. M. Allen and P. R. Cullis, *Science*, 2004, **303**, 1818–1822
- H. Maeda, H. Nakamura and J. Fang, *Adv. Drug Deliv. Rev.*, 2013, **65**, 71–79
- J. Nicolas, S. Mura, D. Brambilla, N. Mackiewicz and P. Couvreur, *Chem. Soc. Rev.*, 2013, **42**, 1147–1235
- S. Mura, J. Nicolas and P. Couvreur, *Nat. Mater.*, 2013, **12**, 991–1003
- R. Duncan, *Nat. Rev. Drug Discov.*, 2003, **2**, 347–360
- A. S. Hoffman, *Adv. Drug Deliv. Rev.*, 2013, **65**, 10–16
- V. P. Torchilin, *Nat. Rev. Drug Discov.*, 2014, **13**, 813–827

- 9 J. Liu, Y. Huang, A. Kumar, A. Tan, S. Jin and A. Mozhi, *Biotechnol. Adv.*, 2014, **32**, 693–710
- 10 H. Cabral, N. Nishiyama and K. Kataoka, *Acc. Chem. Res.*, 2011, **44**, 999–1008
- 11 A. Joseph, C. Contini, D. Cecchin, S. Nyberg, L. Ruiz-Perez, J. Gaitzsch, G. Fullstone, X. Tian, J. Azizi, J. Preston, G. Volpe and G. Battaglia, *Sci. Adv.*, 2017, **3**, e1700362
- 12 J. Li, A. Dirisala, Z. Ge, Y. Wang, W. Yin, W. Ke, K. Toh, J. Xie, Y. Matsumoto, Y. Anraku, K. Osada and K. Kataoka, *Angew. Chemie*, 2017, **129**, 14213–14218
- 13 K. Zhu, G. Liu, J. Hu and S. Liu, *Biomacromolecules*, 2017, **18**, 2571–2582
- 14 Z. Deng, Y. Qian, Y. Yu, G. Liu, J. Hu, G. Zhang and S. Liu, *J. Am. Chem. Soc.*, 2016, **138**, 10452–10466
- 15 Y. Xiao, H. Sun and J. Du, *J. Am. Chem. Soc.*, 2017, **139**, 7640–7647
- 16 H.-S. Peng and D. T. Chiu, *Chem. Soc. Rev.*, 2015, **44**, 4699–4722
- 17 J. Yin, Y. Hu and J. Yoon, *Chem. Soc. Rev.*, 2015, **44**, 4619–4644
- 18 K. Zhou, H. Liu, S. Zhang, X. Huang, Y. Wang, G. Huang, B. D. Sumer and J. Gao, *J. Am. Chem. Soc.*, 2012, **134**, 7803–7811
- 19 J. Madsen, I. Canton, N. J. Warren, E. Themistou, A. Blanz, B. Ustbas, X. Tian, R. Pearson, G. Battaglia, A. L. Lewis and S. P. Armes, *J. Am. Chem. Soc.*, 2013, **135**, 14863–14870
- 20 X. Wang, J. A. Stolwijk, T. Lang, M. Sperber, R. J. Meier, J. Wegener and O. S. Wolfbeis, *J. Am. Chem. Soc.*, 2012, **134**, 17011–17014
- 21 A. M. Breul, M. D. Hager and U. S. Schubert, *Chem. Soc. Rev.*, 2013, **42**, 5366–5407
- 22 A. B. Mabire, M. P. Robin, W.-D. Quan, H. Willcock, V. G. Stavros and R. K. O'Reilly, *Chem. Commun.*, 2015, **51**, 9733–9736
- 23 A. B. Mabire, Q. Brouard, A. Pitto-Barry, R. J. Williams, H. Willcock, N. Kirby, E. Chapman and R. K. O'Reilly, *Polym. Chem.*, 2016, **7**, 5943–5948
- 24 O. S. Wolfbeis, *Chem. Soc. Rev.*, 2015, **44**, 4743–4768
- 25 W. Shi and H. Ma, *Chem. Commun.*, 2012, **48**, 8732–8744
- 26 E. Oliveira, E. Bértolo, C. Núñez, V. Pilla, H. M. Santos, J. Fernández-Lodeiro, A. Fernández-Lodeiro, J. Djafari, J. L. Capelo and C. Lodeiro, *ChemistryOpen*, 2017, **7**, 9–52.
- 27 J. Hu, G. Zhang, Z. Ge and S. Liu, *Prog. Polym. Sci.*, 2014, **39**, 1096–1143
- 28 R. T. Pearson, N. J. Warren, A. L. Lewis and S. P. Armes, *Macromolecules*, 2013, **46**, 1400–1407
- 29 I. Canton and G. Battaglia, *Chem. Soc. Rev.*, 2012, **41**, 2718–2739
- 30 A. L. Harris, *Nat. Rev. Cancer*, 2002, **2**, 38–47
- 31 I. Canton, M. Massignani, N. Patikarnmonthon, L. Chierico, J. Robertson, S. A. Renshaw, N. J. Warren, J. P. Madsen, S. P. Armes, A. L. Lewis and G. Battaglia, *FASEB J.*, 2013, **27**, 98–108
- 32 H. Lomas, M. Massignani, K. a. Abdullah, I. Canton, C. Lo Presti, S. MacNeil, J. Du, A. Blanz, J. Madsen, S. P. Armes, A. L. Lewis and G. Battaglia, *Faraday Discuss.*, 2008, **139**, 143–159
- 33 J. Jose and K. Burgess, *Tetrahedron*, 2006, **62**, 11021–11037.
- 34 H. E. Colley, V. Hearnden, M. Avila-Olias, D. Cecchin, I. Canton, J. Madsen, S. Macneil, N. Warren, K. Hu, J. A. McKeating, S. P. Armes, C. Murdoch, M. H. Thornhill and G. Battaglia, *Mol. Pharm.*, 2014, **11**, 1176–1188
- 35 V. Ladmiral, M. Semsarilar, I. Canton and S. P. Armes, *J. Am. Chem. Soc.*, 2013, **135**, 13574–13581
- 36 L. P. D. Ratcliffe, A. J. Ryan and S. P. Armes, *Macromolecules*, 2013, **46**, 769–777
- 37 I. Canton, N. J. Warren, A. Chahal, K. Amps, A. Wood, R. Weightman, E. Wang, H. Moore and S. P. Armes, *ACS Cent. Sci.*, 2016, **2**, 65–74
- 38 R. Narain and S. P. Armes, *Biomacromolecules*, 2003, **4**, 1746–1758
- 39 L. P. D. Ratcliffe, K. J. Bentley, R. Wehr, N. J. Warren, B. R. Saunders and S. P. Armes, *Polym. Chem.*, 2017, **8**, 5962–5971
- 40 L. Ruiz-Pérez, J. Madsen, E. Themistou, J. Gaitzsch, L. Messenger, S. P. Armes and G. Battaglia, *Polym. Chem.*, 2015, **6**, 2065–2068
- 41 M. A. Gauthier, M. I. Gibson and H.-A. Klok, *Angew. Chemie Int. Ed.*, 2009, **48**, 48–58
- 42 W. L. A. Brooks and B. S. Sumerlin, *Chem. Rev.*, 2016, **116**, 1375–1397
- 43 V. J. Cunningham, A. M. Alswieleh, K. L. Thompson, M. Williams, G. J. Leggett, S. P. Armes and O. M. Musa, *Macromolecules*, 2014, **47**, 5613–5623
- 44 R. Deng, Y. Ning, E. R. Jones, V. J. Cunningham, N. J. W. Penfold, S. P. Armes, G. Fung, K. S. Lam, K. Sakurai, J. Zhao, T. D. James, S. Zauscher, I. Luzinov and S. Minko, *Polym. Chem.*, 2017, **128**, 4226–4227
- 45 R. Deng, M. J. Derry, C. J. Mable, Y. Ning and S. P. Armes, *J. Am. Chem. Soc.*, 2017, **139**, 7616–7623
- 46 S. V. Ley, D. K. Baeschlin, D. J. Dixon, A. C. Foster, S. J. Ince, H. W. M. Priepeke and D. J. Reynolds, *Chem. Rev.*, 2001, **101**, 53–80
- 47 Z.-H. Xu, C. R. McArthur and C. C. Leznoff, *Can. J. Chem.*, 1983, **61**, 1405–1409
- 48 A. Akelah and D. C. Sherrington, *Chem. Rev.*, 1981, **81**, 557–587
- 49 W. Chen, H. Yang, R. Wang, R. Cheng, F. Meng, W. Wei and Z. Zhong, *Macromolecules*, 2010, **43**, 201–207
- 50 C. Pietsch, A. Vollrath, R. Hoogenboom and U. S. Schubert, *Sensors*, 2010, **10**, 7979–7990
- 51 O. a. Khakhel, *J. Appl. Spectrosc.*, 2001, **68**, 280–286
- 52 X. Zhang, X. Zhang, L. Tao, Z. Chi, J. Xu and Y. Wei, *J. Mater. Chem. B*, 2014, **2**, 4398–4414
- 53 Z. Huang, X. Zhang, X. Zhang, C. Fu, K. Wang, J. Yuan, L. Tao and Y. Wei, *Polym. Chem.*, 2015, **6**, 607–612
- 54 Y. Hong, J. W. Y. Lam and B. Z. Tang, *Chem. Commun.*, 2009, **29**, 4332–4353
- 55 P. V. Kreller, David I., Kamat, *J. Phys. Chem.*, 1991, **95**, 4406–4410
- 56 S. J. Isak and E. M. Eyring, *J. Photochem. Photobiol. A Chem.*, 1992, **64**, 343–358
- 57 M. Urrutia and C. Ortiz, *Biotech Histochem*, 2014, **295**, 1–8
- 58 Q. Wan, Y. Song, Z. Li, X. Gao and H. Ma, *Chem. Commun.*, 2013, **49**, 502–504.
- 59 Q.-Q. Wan, X.-H. Gao, X.-Y. He, S.-M. Chen, Y.-C. Song, Q.-Y. Gong, X.-H. Li and H.-M. Ma, *Chem. Asian J.*, 2014, **9**, 2058–2062
- 60 E. Oliveira, C. I. M. Santos, H. M. Santos and A. Fernández-Lodeiro, *Dye. Pigment.*, 2014, **110**, 219–226
- 61 M. Save, J. V. M. Weaver, S. P. Armes and P. McKenna, *Macromolecules*, 2002, **35**, 1152–1159.
- 62 B. S. Beckingham, G. E. Sanoja and N. A. Lynd, *Macromolecules*, 2015, **48**, 6922–6930
- 63 K. Skrabania, A. Miasnikova, A. M. Bivigou-Koumba, D. Zehm and A. Laschewsky, *Polym. Chem.*, 2011, **2**, 2074–2083
- 64 P. Yang, O. O. Mykhaylyk, E. R. Jones and S. P. Armes, *Macromolecules*, 2016, **49**, 6731–6742
- 65 G. Basu Ray, I. Chakraborty and S. P. Moulik, *J. Colloid Interface Sci.*, 2006, **294**, 248–254
- 66 G. K. Bains, S. H. Kim, E. J. Sorin and V. Narayanaswami, *Biochemistry*, 2012, **51**, 6207–6219.
- 67 G. Bains, A. B. Patel and V. Narayanaswami, *Molecules*, 2011, **16**, 7909–7935
- 68 A. Jäger, E. Jäger, F. Surman, A. Höcherl, B. Angelov, K. Ulbrich, M. Drechsler, V. M. Garamus, C. Rodriguez-Emmenegger, F. Nallet and P. Štěpánek, *Polym. Chem.*, 2015, **6**, 4946–4954
- 69 Y. Q. Hu, M. S. Kim, B. S. Kim and D. S. Lee, *Polymer*, 2007, **48**, 3437–3443

- 70 C. H. Bamford and E. F. T. White, *Trans. Faraday Soc.*, 1956, **52**, 716–727
- 71 N. K. Das and B. M. Mandal, *Polymer*, 1982, **23**, 1653–1658
- 72 M. Lucarini, P. Pedrielli, G. F. Pedulli, L. Valgimigli, D. Gigmes and P. Tordo, *J. Am. Chem. Soc.*, 1999, **121**, 11546–11553
- 73 M. Grabolle, R. Brehm, J. Pauli, F. M. Dees, I. Hilger and U. Resch-Genger, *Bioconjug. Chem.*, 2012, **23**, 287–292
- 74 S. Perrier, P. Takolpuckdee and C. A. Mars, *Macromolecules*, 2005, **38**, 2033–2036
- 75 H. Willcock and R. K. O'Reilly, *Polym. Chem.*, 2010, **1**, 149–157
- 76 M. J. S. Dewar and R. C. Dougherty, *The PMO Theory of Organic Chemistry*, Plenum Press, New York, **1st edn.**, 1975
- 77 Y. Wei, R. Hariharan and S. a. Patel, *Macromolecules*, 1990, **23**, 758–764
- 78 V. Martinez and M. Henary, *Chem. - A Eur. J.*, 2016, **22**, 13764–13782
- 79 S. Fery-forgues and D. Lavabre, *J. Chem. Educ.*, 1999, **76**, 1260–1264
- 80 S. J. Isak and E. M. Eyring, *J. Phys. Chem.*, 1992, **58**, 1738–1742
- 81 A. Jafari, A. Ghanadzadeh, H. Tajalli, M. Yeganeh and M. Moghadam, *Spectrochim. Acta - Part A Mol. Biomol. Spectrosc.*, 2007, **66**, 717–725
- 82 Y. Ma, Y. Tang, N. C. Billingham, S. P. Armes and A. L. Lewis, *Biomacromolecules*, 2003, **4**, 864–868
- 83 H. Lomas, A. P. R. Johnston, G. K. Such, Z. Zhu, K. Liang, M. P. van Koeverden, S. Alongkornchotikul and F. Caruso, *Small*, 2011, **7**, 2109–2019
- 84 J. Du, Y. Tang, A. L. Lewis and S. P. Armes, *J. Am. Chem. Soc.*, 2005, **127**, 17982–17983
- 85 C. Giacomelli, L. Le Men, R. Borsali, J. Lai-Kee-Him, A. Brisson, S. P. Armes and A. L. Lewis, *Biomacromolecules*, 2006, **7**, 817–828
- 86 H. Lomas, J. Du, I. Canton, J. Madsen, N. Warren, S. P. Armes, A. L. Lewis and G. Battaglia, *Macromol. Biosci.*, 2010, **10**, 513–530
- 87 J. N. Israelachvili, D. J. Mitchell and B. W. Ninham, *J. Chem. Soc. Faraday Trans. 2*, 1976, **72**, 1525–1568.
- 88 A. Lambacher and P. Fromherz, *Appl. Phys. A Mater. Sci. Process.*, 1996, **63**, 207–216.